# Ultrasmooth and Thermally Stable Silver-Based Thin Films with Subnanometer Roughness by Aluminum Doping

**Deen Gu,[†,‡,§] Cheng Zhang,[†,§] Yi-Kuei Wu,[†] and L. Jay Guo*[,†]**

[†]Department of Electrical Engineering and Computer Science, University of Michigan, Ann Arbor, Michigan 48109, United States, and [‡]School of Optoelectronic Information, University of Electronic Science and Technology of China, Chengdu, Sichuan 610054, People's Republic of China. [§]D. Gu and C. Zhang contributed equally.

**ABSTRACT** Rough surface and poor stability of ultrathin Ag films limit their applications in nanophotonic and optoelectronic devices. Here, we report an approach for fabricating ultrasmooth and thermally stable Ag-based thin films on $SiO_2$/Si substrates by Al-doping. The effect of Al-doping on the surface morphology and stability of ultrathin Ag films at room temperature and elevated temperature was investigated. The 15 nm Al-doped Ag films with an Al atomic concentration of 4% have a root-mean-square roughness as low as 0.4 nm. The smooth surface morphology is maintained even after 300 °C annealing in $N_2$. Al-doping enhances the nuclei density of films. Moreover, a capping layer spontaneously formed over the Al-doped Ag films restrains the surface diffusion and mass transportation of Ag atoms. Therefore, Al-doping induces ultrathin Ag films with highly stable and ultrasmooth surface morphology.

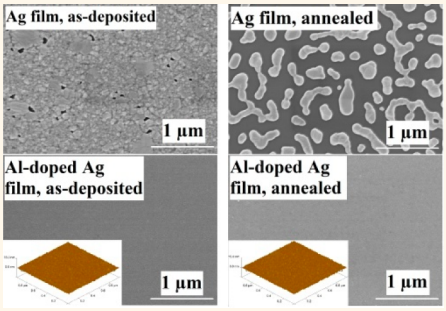


**KEYWORDS:** Ag films · Al-doping · ultrasmoothness · thermal stability · RMS roughness · capping layer

Ag is one of the most important and frequently employed metal materials for plasmonic devices, metamaterials, and other optoelectronic applications due to relatively low loss in the visible and NIR regions compared to other metals.[1,2] However, Ag films tend to grow in Vomer–Webber mode on dielectric substrates,[3−5] which causes a rough surface on the Ag films. Especially, many applications require very thin Ag films (*e.g.*, metamaterials in the form of metal–dielectric stacks[6]), but the Ag film becomes discontinuous when the nominal thickness of the Ag layer is less than 10 nm.[7] Often the rough surface is detrimental to high-quality and low-loss nanophotonic devices due to significant scattering loss and degraded performance from the inhomogeneity of the thickness.[8−10] Thus, achieving thin and smooth Ag films is crucial for many nanophotonic applications. Previously, by using a 1−2 nm Ge nucleation layer, smooth Ag films with about 0.6 nm root-mean-square (RMS) surface roughness were realized.[11,12] However, Ge is a low-band-gap semiconductor and has strong absorption in the visible range,[13] which is not desirable for low-loss optical elements. A Ni seed layer was also used to deposit smooth Ag films,[5] but was not as effective as using the Ge wetting layer. Other seed layers, such as Cu,[14] Nb,[4] $MoO_3$,[7] and poly(3,4-ethylene dioxythiophene):poly(styrenesulfonate) (PEDOT:PSS),[15] have also been shown to reduce the surface roughness of Ag films. It is noteworthy that using a seed layer is generally undesirable for the performance of plasmonic devices due to the damping by the seed layer.[16,17] A template-stripping procedure is another attractive technique for fabricating ultrasmooth Ag films.[9,18,19] This technique is promising for the wafer-scale fabrication of high-quality plasmonic devices with smooth patterned surfaces due to low-cost and high-throughput production.[20−23] However, for metal–dielectric multilayer structures it will still face the challenge of rough metal layers deposited on the dielectric layers. Very recently, a novel two-step process (low-temperature epitaxial deposition followed by room-temperature annealing) combined with a thin capping

* Address correspondence to guo@umich.edu.

Received for review July 2, 2014 and accepted September 11, 2014.

**Published online September 11, 2014**
**10.1021/nn503577c**

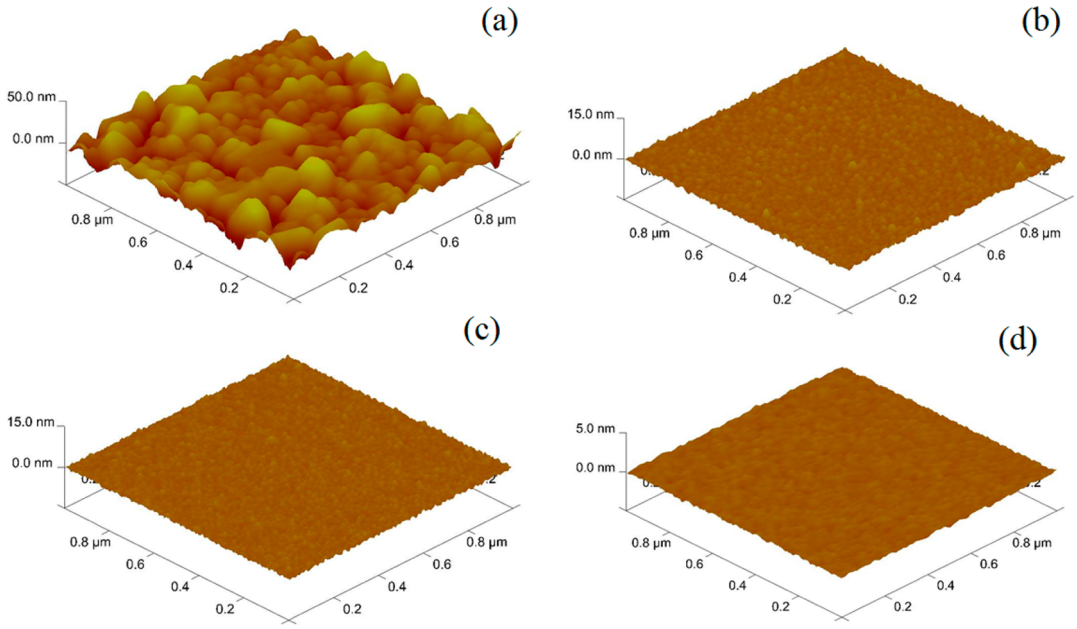


**Figure 1. Representative surface morphologies by AFM for (a) 15 nm pure Ag film on $SiO_2$/Si(100), (b) 15 nm Al-doped Ag (AA-130) film on $SiO_2$/Si(100), (c) 6 nm AA-130 film on $SiO_2$/Si(100), and (d) $SiO_2$/Si(100) substrate. The 15 nm Ag film has an RMS roughness of 6.87 nm, which is about 16 times larger than the 15 nm Al-doped Ag (AA-130) film (0.43 nm). The 6 nm AA-130 film has a RMS roughness of 0.37 nm, and the RMS roughness of a $SiO_2$/Si(100) substrate is 0.10 nm.**

dielectric layer has successfully produced Ag films with atomically smooth surface morphology on a Si(111) substrate.[8] But this process is relatively time-consuming and of high cost, due to the requirement of a more elaborate process and specialized equipment.

The poor stability of thin Ag films and the associated nanostructures is another barrier for many practical applications.[24−26] Dewetting occurs spontaneously on the dielectric substrate even at room temperature especially for ultrathin Ag films.[8,27,28] Atomically flat ultrathin Ag films tend to transform to 3D islands for the Ag/dielectric nonwetting system.[29] This dewetting tendency becomes more obvious at elevated temperature.[28,30−32] Dewetting has been observed even for 35 nm thick Ag films on $SiO_2$ when the temperature exceeds 102 °C.[32] In order to improve the stability of Ag films, adding an adhesion layer is a common strategy.[16,26,33] However, the detrimental effects of an adhesion layer on the performance of plasmonic devices have been reported.[16] Another approach is to add a capping layer to stabilize the Ag films.[34,35] An oxide layer ($SiO_2$, $Cr_2O_3$, *etc.*) with thickness of tens of nanometers can inhibit the agglomeration of Ag films at elevated temperature. Very recently, a simple synthetic protocol has been reported to obtain ultrastable silver nanoparticles by forming a silver thiolate protecting layer, which greatly enhances the stability of Ag nanoclusters.[24] Another interesting strategy to stabilize the Ag nanostructures is using UV irradiation to induce the reconstruction of Ag nanoplates.[25] However, the thermal stability of these Ag nanostructures was not evaluated at elevated temperatures.

In this paper, a simple and effective approach is demonstrated for fabricating ultrasmooth Ag-based thin films with both a subnanometer RMS roughness and high thermal stability. The two key features are achieved by introducing a small amount of Al into Ag during a simple co-deposition process.[39] The RMS roughness of a 15 nm Al-doped Ag film is as low as 0.4 nm. The RMS roughness and surface morphology of the ultrasmooth film remain essentially unchanged even after annealing at 300 °C.

## RESULTS AND DISCUSSION

**Surface Morphology of Al-Doped Ag Ultrathin Films.** Figure 1 shows the atomic force microscope (AFM) images of the surface morphology of a 15 nm pure Ag film and 6 and 15 nm Al-doped Ag films, deposited by using the sputtering power of 130 W for an Al target and 200 W for a Ag target (denoted as AA-130), on $SiO_2$/Si(100) over a scan size of 1 $\mu$m × 1 $\mu$m. As a reference, the surface morphology of a $SiO_2$/Si(100) substrate is shown in Figure 1c. The pure Ag film on $SiO_2$/Si(100) is very rough, with an RMS roughness of 6.87 nm. In high contrast, the Al-doped Ag film is much smoother than the pure Ag film, with a RMS roughness of only 0.43 nm (Figure 1b). The height histogram indicates the peak-to-valley height difference and the deviation from the average surface-height value. These are shown in Figure S1a′−d′, which correspond to the AFM images shown in Figure 1a−d. The peak-to-valley height of the pure Ag film has a wide distribution, with the average value of 25.6 nm and the maximum value of 48.9 nm, which is consistent with the measured rough surface morphology. The Al-doped Ag film has a narrow peak-to-valley height distribution,

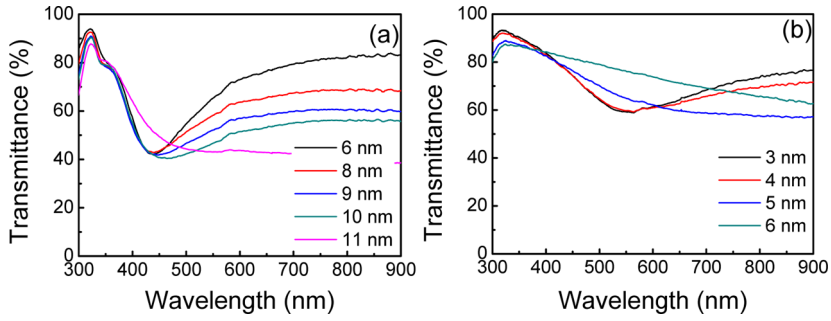


**Figure 2. Transmittance spectra of (a) pure Ag films and (b) Al-doped Ag (AA-130) films with different thicknesses.**

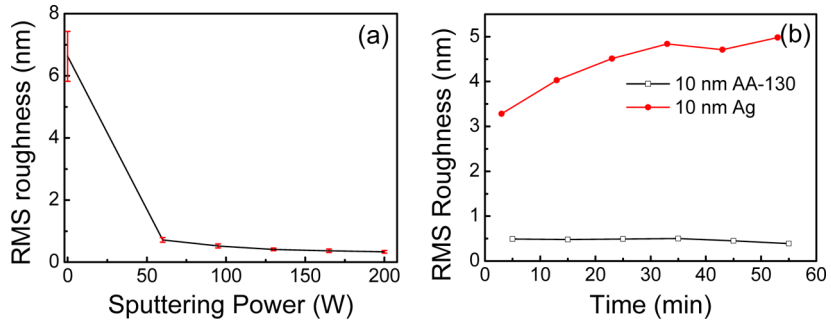


**Figure 3. (a) RMS roughness of Al-doped Ag films co-deposited by the different sputtering power of an Al target with 200 W power of a Ag target. (b) Evolution of RMS roughness of a 10 nm pure Ag film and a 10 nm AA-130 film with time under ambient atmosphere at room temperature.**

with an average value of 3.1 nm and a maximum value of 4.5 nm. This further demonstrates the ultrasmooth surface morphology of the Al-doped Ag film.

Al-doping not only results in ultrasmooth surface morphology but also greatly reduces the percolation threshold of forming a continuous film from 11 nm for pure Ag films to 6 nm for Al-doped Ag films, according to the results from electrical measurement and optical measurement. Pure Ag films are highly resistive (sheet resistance >450 kΩ·sq$^{-1}$, limited by the measurement range of the four-point probe used (Miller FPP-5000)) due to the discontinuity of the film until the thickness reaches 11 nm. In comparison, the AA-130 film becomes highly conductive at a thickness of 6 nm (Table S1). Moreover, at 6 nm, the surface of Al-doped Ag films remains smooth, as shown in Figure 1c. Figure 2 shows the transmittance spectra of pure Ag films and AA-130 films with different thicknesses deposited on fused silica substrates by using a UV−vis−NIR spectrometer. There is a broad dip for the pure Ag and AA-130 films when the thickness is less than the percolation threshold. This originates from the localized surface plasmon resonance (LSPR) of electrically discontinuous metal island films.[36,37] Once the thickness of the films reaches the percolation threshold and beyond, the reflection increases toward the infrared regime,[38] as is the case of a typical continuous metal film, leading to a gradual decrease in the film transmittance. The 6 nm AA-130 film is highly transparent, with the transmission of over 65% in the whole visible range (400−800 nm). The optical loss in the visible regime of 15 nm annealed Al-doped Ag films is close to that of bulk Ag by comparing the imaginary part of the dielectric function ($\varepsilon_2$) determined from the spectroscopic ellipsometry measurement (Figure S2). Such an ultrathin continuous Al-doped Ag film is very promising for transparent conductor applications (*e.g.*, light-emitting and photovoltaic devices) due to the high transmission and electrical conductivity.[39]

The effect of Al concentration in the film on the surface morphology was evaluated by varying the Al deposition rate, *i.e.*, the sputtering power of the Al target (Figure S3). Figure 3a shows the RMS roughness of the Ag film and Al-doped Ag films deposited with different sputtering power of the Al target. The RMS roughness of the Ag film was drastically decreased from 6.5 nm to 0.7 nm even by introducing a small amount of Al using a 60 W sputtering power for Al. Sixty watts is the lowest power that can sustain a stable glow discharge for the Al target in our current sputtering system. The RMS roughness was further decreased to about 0.4 nm with increasing the sputtering power of the Al target to 130 W, then saturates. This observation reveals that Al-doping remarkably reduces the roughness of Ag films.

**Stability of the Surface Morphologies of Pure Ag Thin Films and Al-Doped Ag Films.** Another interesting observation is that the Al-doped Ag film exhibits drastically improved stability. The effect of Al-doping on the stability of Ag films was evaluated first at room temperature. The RMS roughness for the same region of the 10 nm pure Ag film and AA-130 film under ambient atmosphere at

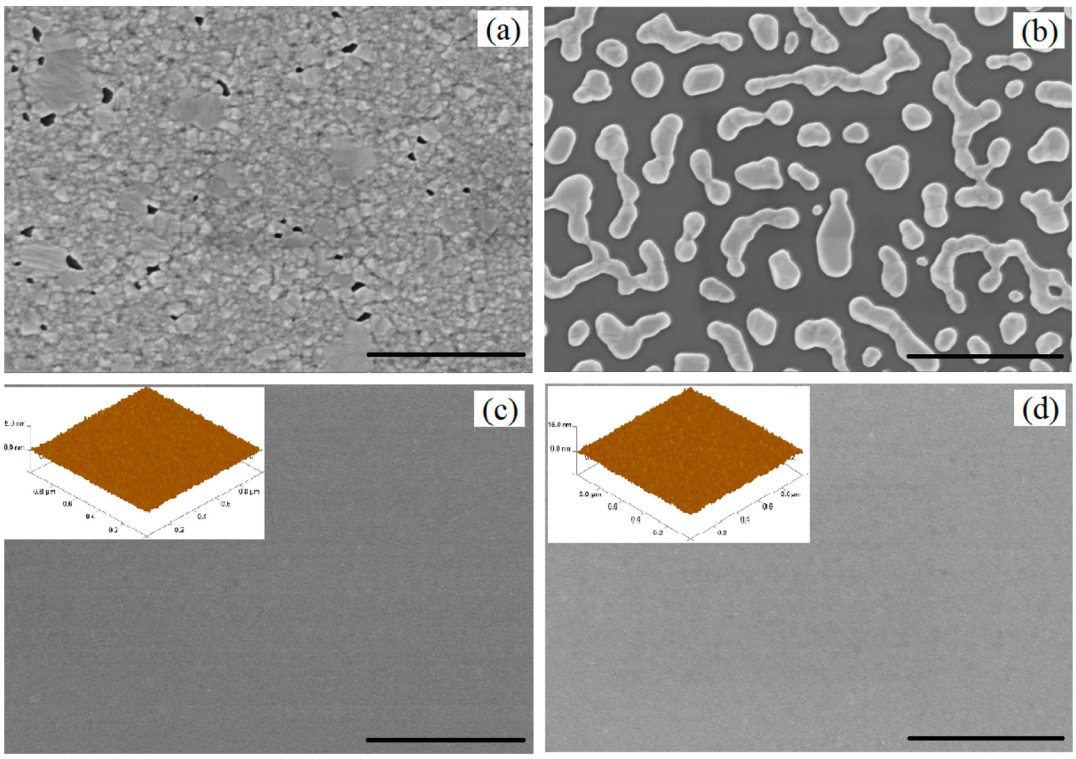


**Figure 4. SEM micrographs (scale bars = 1 $\mu$m) of (a) 15 nm as-deposited and (b) annealed pure Ag films on $SiO_2$/Si in $N_2$ at 300 °C; (c) 15 nm as-deposited and (d) annealed Al-doped Ag films on $SiO_2$/Si in $N_2$ at 300 °C. The insets in (c) and (d) are AFM images of 15 nm as-deposited and annealed Al-doped Ag films on $SiO_2$/Si with an RMS roughness of 0.43 and 0.45 nm, respectively.**

room temperature was characterized by AFM at 5, 15, 25, 35, 45, and 55 min, respectively, after the film deposition, as shown in Figure 3b. The RMS roughness of the 10 nm pure Ag film increases from 3.3 nm to 4.8 nm when the aging time extends from 5 min to 35 min, while there is no obvious change of the RMS roughness for 10 nm AA-130 films even after 55 min. This indicates that quick coalescence occurs for 10 nm pure Ag films within 35 min under ambient atmosphere, while the surface morphology of the 10 nm Al-doped Ag film is very stable under the same condition. The stability difference of the surface morphology between pure Ag films and Al-doped Ag films can be further demonstrated by comparing the 3D AFM surface morphology recorded after 5 min with that from 55 min (Figure S4). It can be clearly observed that Al-doping greatly improves the stability of the surface morphology of Ag films at room temperature.

The effect of Al-doping on the stability of Ag films was also evaluated at elevated temperature. Figure 4 compares the change of surface morphology, characterized by using scanning electron microscopy (SEM), of a 15 nm pure Ag film and a 15 nm AA-130 film after annealing for 15 min in a nitrogen atmosphere at 300 °C. Pure Ag films evolved from a rough, but continuous film (Figure 4a) into isolated islands (Figure 4b) after annealing due to dewetting,[32] which is a typical behavior for pure Ag films on a dielectric substrate at elevated temperature.[27,30] In contrast, the 15 nm annealed AA-130 film shows a very similar ultrasmooth surface morphology to the as-deposited one (Figure 4c and Figure 4d). AFM images (shown as the insets in Figure 4c and d) further demonstrate that there is no obvious difference in the surface morphology and RMS roughness before and after the annealing. These results reveal that Al-doping results in outstandingly thermally stable and ultrasmooth Ag-based films, which provides a promising opportunity for many nanophotonic devices requiring ultrasmooth surface morphology and relatively high-temperature processes.[40]

**Mechanisms for Ultrasmooth and High Thermally Stable Surface Morphology of Al-Doped Ag Thin Films.** The ultrasmooth surface morphology and lower percolation threshold of Al-doped Ag films indicate that a small amount of Al may strongly influence the nucleation and subsequent growth of Ag films on an oxide substrate.[41] In order to investigate the effect of Al-doping on the nuclei density of Ag films, the surface morphology of pure Ag and AA-130 films with a nominal thickness of 3 nm was measured by AFM. Figure 5a and b obviously show that Al-doping results in smaller and denser particles than those in the pure Ag films. This reveals that Al-doping causes an increase in the nuclei density of the films. The nuclei density and particle size of metal films are related to the diffusion

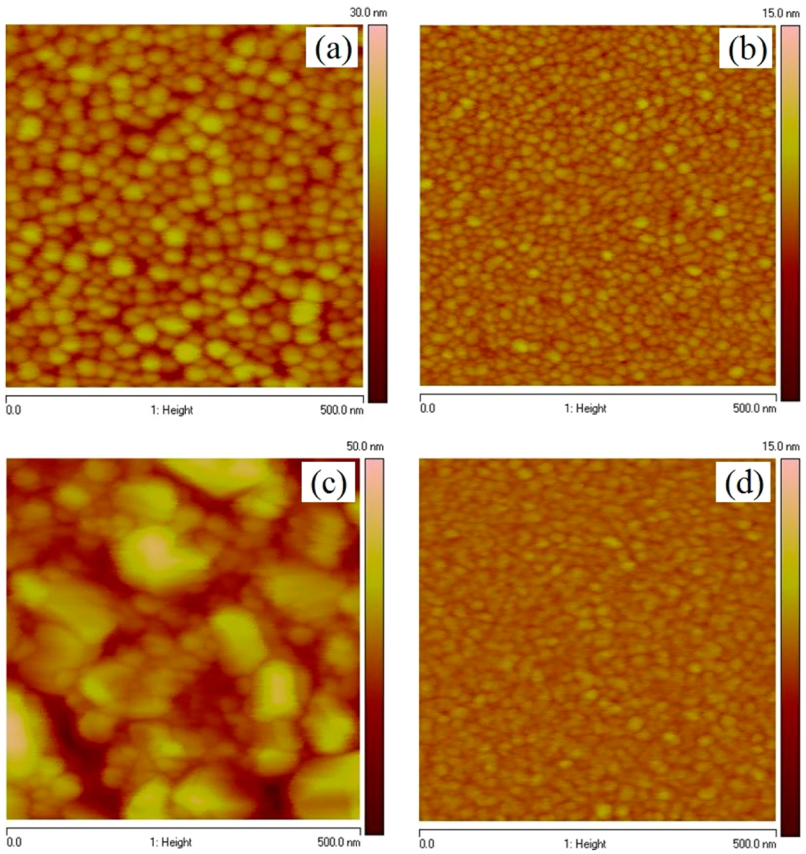


**Figure 5. 2D AFM images of (a) 3 nm pure Ag films, (b) 3 nm Al-doped Ag films, (c) 15 nm pure Ag films, and (d) 15 nm Al-doped Ag films on $SiO_2$/Si(100) substrates.**

rate of the metal atoms on the dielectric surface.[11,42] The metals with smaller diffusion rate on the surface exhibit higher nuclei density and smaller particle size. The diffusion rate of the metal atoms on oxide substrates generally decreases with an increase in the metal−oxygen bond strength.[3,42,43] The bond strength of Al−O bonds is much larger than that of Ag−O bonds.[3] As a result, the average diffusion distance of Al atoms on the surface of $SiO_2$ is smaller than that of Ag atoms, and Al atoms are easier to be immobilized on the surface of $SiO_2$ than Ag due to stronger bonding with the oxidized surface. Therefore, Al-doping results in an enhanced density of heterogeneous nucleation sites, and thus larger nuclei density and smaller particle size.

The effect of Al-doping on the subsequent growth of Ag films was also evaluated by comparing the surface morphologies of the nucleation layer (Figure 5a and b) with those of 15 nm thick films for both pure Ag films (Figure 5c) and AA-130 films (Figure 5d), respectively. Table S2 lists the quantitative parameters of the surface morphologies shown in Figure 5. For pure Ag films, due to the high mobility of Ag atoms, the small particles coalesce into larger ones during the film growth from 3 nm to 15 nm, leading to increased RMS roughness. Different from pure Ag films, the particle size of AA-130 films is slightly increased from 15−25 nm to 25−30 nm when the thickness increases from 3 nm to 15 nm. Moreover, the surface morphology became even smoother. These results indicate that the existence of Al in Ag films reduces the surface diffusion and mass transportation of Ag atoms and restrains the expansion of the Ag particle size during the film growth.

The results from the X-ray diffraction (XRD) patterns and transmission electron microscope (TEM) analysis further demonstrate that Al-doping effectively curbs the enlarging of the grain size. Figure 6a shows the XRD patterns of 50 nm Al-doped Ag films and pure Ag films. All the diffraction peaks, except the Si(004) peak at 69.68° from the substrate, can be assigned to the cubic Ag (PDF No. 87-0719).[44,45] This means no other phase is introduced into the Ag films due to Al-doping. The average grain sizes for AA-130 and pure Ag thin films, calculated from the full width at half-maximum (fwhm) of the main diffraction peak (111) by the Scherrer equation, are 9.7 and 30.1 nm, respectively. This means that Al-doping remarkably reduces the grain size of Ag films. The selected area diffraction (SAD) pattern for a 15 nm Al-doped Ag film (Figure 6b) exhibits the same series of Debye−Scherrer diffraction rings as 15 nm pure Ag films (Figure 6c), which can both be completely indexed as cubic Ag. Al-doped Ag films have the same crystalline type as pure Ag films. Figure 6d and e

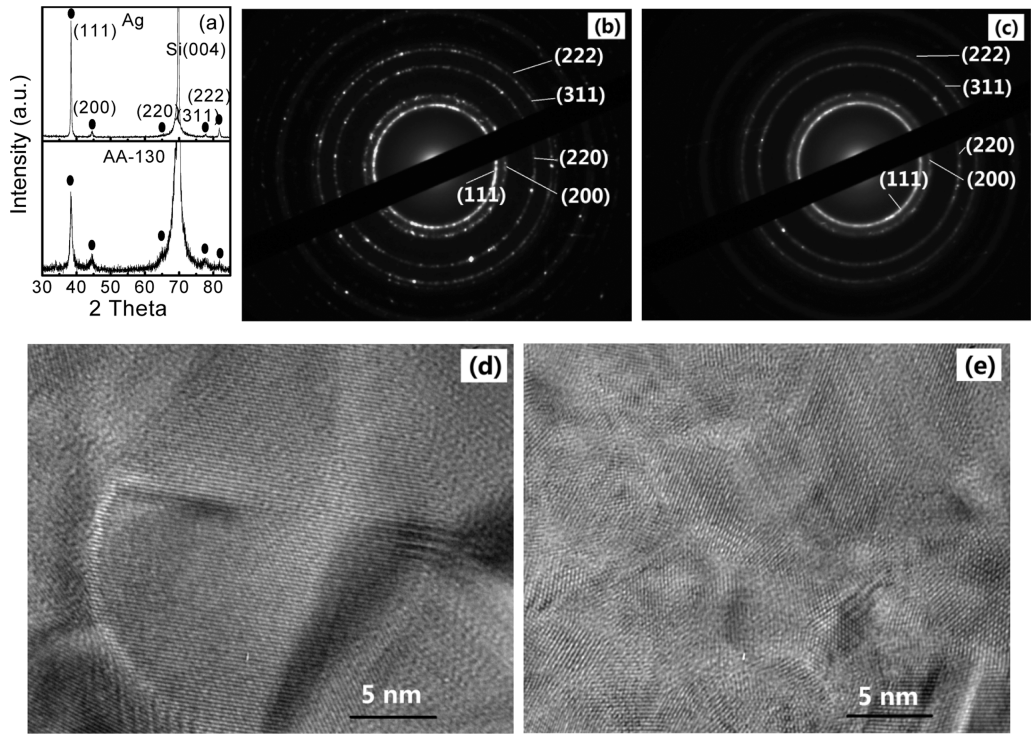


**Figure 6. Structural characterization of thin films: (a) XRD patterns of AA-130 and pure Ag thin films, the SAD patterns of (b) pure Ag and (c) AA-130 thin films, and HRTEM micrographs (scale bars = 5 nm) of (d) pure Ag and (e) AA-130 thin films.**

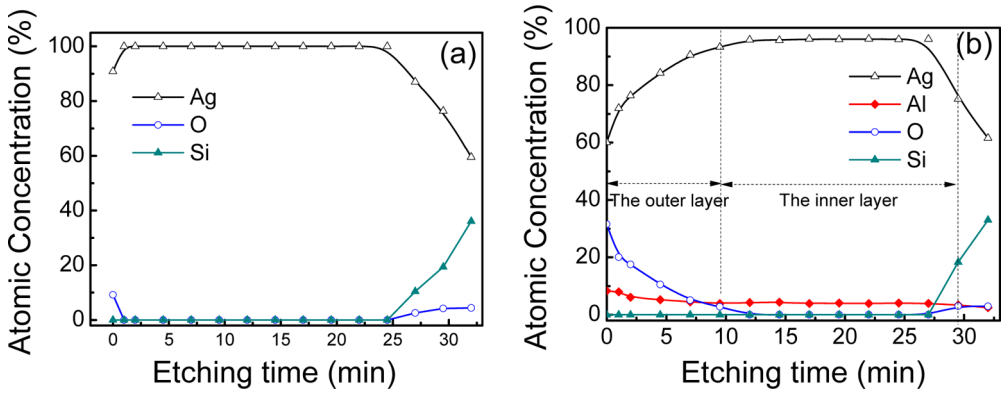


**Figure 7. Composition depth profiles of (a) a 50 nm pure Ag film and (b) a 50 nm AA-130 film.**

are the representative high-resolution TEM (HRTEM) images of 15 nm Al-doped Ag films and pure Ag films. They both reveal clear lattice fringes for cubic Ag crystals. A pure Ag film has a typical grain size of about 30 nm, and an Al-doped Ag film has an average grain size of 9−12 nm, comparable to those from the XRD data.

To investigate how Al-doping restrains the surface diffusion and mass transportation of Ag, depth profiling and analysis of the chemical states of elements were carried out by X-ray photoelectron spectroscopy (XPS). Considering that there are still voids in the 15 nm pure Ag film (as shown in Figure 4a), we used thicker Ag and AA-130 films (50 nm), which can completely cover the surface of the substrate, for XPS analysis.

Figure 7 shows the composition depth profiles of the 50 nm pure Ag film and those of 50 nm AA-130 film. For the 50 nm Ag film, oxygen was detected only at the surface of the as-prepared sample and when reaching the interface between the film and substrate (Figure S5). Close to the interface between the film and substrate, O and Si can be probed after the film is etched for 24.5 min. For the 50 nm AA-130 film, oxygen can be detected from the outer surface of the film and throughout the newly formed surface after 9.5 min of etching, as shown in Figure 7b. Considering that there is no oxygen produced during sputtering, oxygen in Al-doped Ag films should originate from the ambient atmosphere after the samples are taken out of the vacuum. Furthermore, the Al-enriching feature can be clearly observed in the outer layer of AA-130 films (Figure 7b). The atomic concentration of Al drops gradually from about 8% for the outermost surface to

about 4% for the newly formed surface after 9.5 min of etching. After that, the atomic concentration of Al is almost constant at 4% in the inner layer. This implies the outward diffusion of Al together with the inward diffusion of oxygen.

It is well known that Al has a much more negative standard heat of formation of oxides than most metal elements.[3] Therefore, Al tends to be oxidized easily when it is exposed to an oxygen-containing atmosphere.[3] For Al-doped Ag films, oxygen atoms from ambient atmosphere diffused into the film and Al atoms in the film diffused outward, and Al−O bonds were spontaneously formed in order to decrease the free energy of the film system. As a result, Al-doped Ag films consist of two layers: an outer layer containing Al−O bonds with approximately one-third the thickness of the films (estimated from Figure 7b) and an inner layer composed of Ag and Al. Al−O bonds in an outer layer can be further demonstrated by analyzing the chemical state of Al as shown in Figure S6. The existence of Al−O bonds with high stability makes the outer layer act as a capping layer on the Al-doped Ag films. The capping layer restrained the surface diffusion and mass transportation of Ag atoms, which ensures an Al-doped Ag film with a high stability of the ultrasmooth surface morphology at room temperature and even at elevated temperature.

## CONCLUSIONS

We have fabricated ultrasmooth Ag-based thin films by Al-doping through a simple co-sputtering process. Al-doping enhances the nuclei density of films on an oxide surface due to the much larger bond strength of Al−O bonds than Ag−O bonds. The existence of Al in Ag films also causes the inward diffusion of O from the ambient atmosphere and the outward diffusion of Al, thus forming a capping layer containing Al−O bonds with high stability over the Al-doped Ag inner layer. As a result, the Al-doped Ag films have a subnanometer RMS roughness. More importantly, the ultrasmooth surface morphology of Al-doped Ag films remains stable at both room temperature and even at elevated temperature thanks to the spontaneously formed capping layer. This approach provides not only a novel method for transparent conductive films by greatly decreasing the thickness percolation threshold of continuous Ag-based films but also a promising opportunity for many nanophotonic devices requiring ultrasmooth surface morphology and relatively high-temperature processes.

## METHODS

**Film Preparation.** Al-doped Ag films were fabricated by co-sputtering of Ag and Al. The concentration of Al was controlled by varying the sputtering power for the Al target while keeping a constant sputtering power of 200 W for the Ag target. The Al-doped Ag films using a sputtering power of 60, 95, 130, 165, and 200 W for the Al target are denoted as AA-60, AA-95, AA-130, AA-165, and AA-200, respectively. The deposition rate of Ag was calibrated as 0.6 nm/s at 200 W power, and that of Al is 0.06 nm/s at the same power. The film thickness was controlled by the deposition time. The films for AFM, SEM, XPS, and XRD characterization were deposited on $SiO_2$/Si(100) substrates, which were cleaned in acetone and IPA, and dried with nitrogen. Since there is a native oxide layer on the Si wafer, such substrates are referred to as $SiO_2$/Si(100) substrates. The films for optical measurements (transmittance spectra) and electrical measurements were deposited on fused silica substrates.

**Characterization.** The surface morphology of the Al-doped Ag films was investigated using an AFM (Veeco NanoMan) in a tapping mode at ambient conditions and at a scan rate of 0.8 Hz. The AFM images for films were recorded after aging over 12 h except for specified descriptions. The AFM images were analyzed quantitatively by computing the RMS roughness and the peak-to-valley height difference from the topology data.

The conductivity of films was evaluated by measuring the sheet resistance of films using a four-point probe (Miller FPP-5000). The optical losses of thin films were investigated by ellipsometry measurement (J. A. Woollam M-2000). The samples were prepared by deposited 15 nm Al-doped Ag films and Ag films on the silicon substrate with 500 nm thermally oxidized $SiO_2$.

In order to investigate the thermal stability of thin films, the surface morphologies of 15 nm as-prepared and annealed pure Ag and AA-130 thin films were examined by means of SEM (Hitachi SU8000). All the samples were deposited on a $SiO_2$/Si(100) substrate.

The structural characterizations of Al-doped Ag films and pure Ag films were performed by means of XRD and TEM/HRTEM. The XRD patterns were recorded on a Rigaku diffractometer operated at 40 kV with Cu Kα radiation. The thin films with a thickness of 50 nm were used for XRD measurement in order to have enough signal intensity.[46] TEM and HRTEM analyses were executed on 15 nm AA-130 and pure Ag thin films by using the JEOL 3011 TEM facility. TEM samples were prepared by depositing thin films on a copper grid with a $SiO_2$ support film for observation.

XPS (Kratos Axis Ultra XPS) was used to obtain information on the elemental chemical states, atomic concentrations, and the composition depth profiles. The XPS spectra were collected using Al Kα radiation (1486.6 eV), and binding energies were calibrated to the C 1s value at 284.6 eV for adventitious carbon. The depth profiling was performed by recording XPS spectra of the top surface and in the layer depth by $Ar^+$ (4 keV) ion beam sputtering. The XPS concentration depth profiles of silver, oxygen, aluminum, and silicon were calculated from the integrated intensity of the Ag 3d, O 1s, Al 2p, and Si 2p peaks.

*Conflict of Interest:* The authors declare no competing financial interest.

*Supporting Information Available:* Height histograms from the AFM images of films; sheet resistance of thin films; optical losses by the ellipsometry measurement; Al-doping concentrations for varying the sputtering powers of Al target; evolution of the surface morphology recorded by AFM; quantitative data of the surface morphology from the AFM images; analysis of the chemical states by XPS; estimation of the thickness of the outer oxide layer in Al-doped Ag films. This material is available free of charge *via* the Internet at http://pubs.acs.org.

*Acknowledgment.* We acknowledge the technical support of Lurie Nanofabrication Facility (LNF), especially Dr. Pilar Herrera-Fierro and Mr. David Sebastian. We appreciate the support from Electron Microbeam Analysis Laboratory (EMAL), particularly Dr. Haiping Sun, for the film characterization. This work is supported in part by the NSF DMR 1120923. D.G. would like to thank Dr. D. Zhao for helping with AFM and the support

by the National Natural Science Foundation of China (Grant No. 61235006) and the Fundamental Research Funds for the Central Universities (Grant No. ZYGX2012J058).

## REFERENCES AND NOTES


1. Boltasseva, A.; Atwater, H. A. Low-Loss Plasmonic Metamaterials. *Science* **2011**, *331*, 290–291.
2. West, P. R.; Ishii, S.; Naikl, G. V.; Emani, N. K.; Shalaev, V. M.; Boltasseva, A. Searching for Better Plasmonic Materials. *Laser Photonics Rev.* **2010**, *4*, 795–808.
3. Campbell, C. T. Ultrathin Metal Films and Particles on Oxide Surfaces: Structural, Electronic and Chemisorptive Properties. *Surf. Sci. Rep.* **1997**, *27*, 1–111.
4. Anders, A.; Byon, E.; Kim, D. H.; Fukuda, K.; Lim, S. H. N. Smoothing of Ultrathin Silver Films by Transition Metal Seeding. *Solid State Commun.* **2006**, *140*, 225–229.
5. Liu, H.; Wang, B.; Leong, E. S. P.; Yang, P.; Zong, Y.; Si, G. Y.; Teng, J. H.; Maier, S. A. Enhanced Surface Plasmon Resonance on a Smooth Silver Film with a Seed Growth Layer. *ACS Nano* **2010**, *4*, 3139–3146.
6. Xu, T.; Agrawal, A.; Abashin, M.; Chau, K. J.; Lezec, H. J. All-Angle Negative Refraction and Active Flat Lensing of Ultraviolet Light. *Nature* **2013**, *497*, 470–474.
7. Sergeant, N. P.; Hadipour, A.; Niesen, B.; Cheyns, D.; Heremans, P.; Peumans, P.; Rand, B. P. Design of Transparent Anodes for Resonant Cavity Enhanced Light Harvesting in Organic Solar Cells. *Adv. Mater.* **2012**, *24*, 728–732.
8. Lu, Y. J.; Kim, J. S.; Chen, H. Y.; Wu, C. H.; Dabidian, N.; Sanders, C. E.; Wang, C. Y.; Lu, M. Y.; Li, B. H.; Qiu, X. G.; *et al*. Plasmonic Nanolaser Using Epitaxially Grown Silver Film. *Science* **2012**, *337*, 450–453.
9. Nagpal, P.; Lindquist, N. C.; Oh, S.-H.; Norris, D. J. Ultrasmooth Patterned Metals for Plasmonics and Metamaterials. *Science* **2009**, *325*, 594–597.
10. Kim, S. K.; Ee, H. S.; Choi, W.; Kwon, S. H.; Kang, J. H.; Kim, Y. H.; Kwon, H.; Park, H. G. Surface-Plasmon-Induced Light Absorption on a Rough Silver Surface. *Appl. Phys. Lett.* **2011**, *98*, 011109.
11. Logeeswaran, V. J.; Kobayashi, N. P.; Islam, M. S.; Wu, W.; Chaturvedi, P.; Fang, N. X.; Wang, S. Y.; Williams, R. S. Ultrasmooth Silver Thin Films Deposited with a Germanium Nucleation Layer. *Nano Lett.* **2009**, *9*, 178–182.
12. Chen, W.; Chen, K. P.; Thoreson, M. D.; Kildishev, A. V.; Shalaev, V. M. Ultrathin, Ultrasmooth, and Low-Loss Silver Films *via* Wetting and Annealing. *Appl. Phys. Lett.* **2010**, *97*, 211107.
13. Kats, M. A.; Blanchard, R.; Genevet, P.; Capasso, F. Nanometre Optical Coatings Based on Strong Interference Effects in Highly Absorbing Media. *Nat. Mater.* **2013**, *12*, 20–24.
14. Formica, N.; Ghosh, D. S.; Carrilero, A.; Chen, T. L.; Simpson, R. E.; Pruneri, V. Ultrastable and Atomically Smooth Ultrathin Silver Films Grown on a Copper Seed Layer. *ACS Appl. Mater. Interfaces* **2013**, *5*, 3048–3053.
15. Ke, L.; Lai, S. C.; Liu, H.; Peh, C. K. N.; Wang, B.; Teng, J. H. Ultrasmooth Silver Thin Film on PEDOT:PSS Nucleation Layer for Extended Surface Plasmon Propagation. *ACS Appl. Mater. Interfaces* **2012**, *4*, 1247–1253.
16. Siegfried, T.; Ekinci, Y.; Martin, O. J. F.; Sigg, H. Engineering Metal Adhesion Layers That Do Not Deteriorate Plasmon Resonances. *ACS Nano* **2013**, *7*, 2751–2757.
17. Jiao, X. J.; Goeckeritz, J.; Blair, S.; Oldham, M. Localization of Near-Field Resonances in Bowtie Antennae: Influence of Adhesion Layers. *Plasmonics* **2009**, *4*, 37–50.
18. Vogel, N.; Zieleniecki, J.; Köper, I. As Flat as It Gets: Ultrasmooth Surfaces from Template-Stripping Procedures. *Nanoscale* **2012**, *4*, 3820–3832.
19. Lindquist, N. C.; Johnson, T. W.; Norris, D. J.; Oh, S.-H. Monolithic Integration of Continuously Tunable Plasmonic Nanostructures. *Nano Lett.* **2011**, *11*, 3526–3530.
20. Im, H.; Lee, S. H.; Wittenberg, N. J.; Johnson, T. W.; Lindquist, N. C.; Nagpal, P.; Norris, D. J.; Oh, S.-H. Template-Stripped Smooth Ag Nanohole Arrays with Silica Shells for Surface Plasmon Resonance Biosensing. *ACS Nano* **2011**, *5*, 6244–6253.
21. Cherukulappurath, S.; Johnson, T. W.; Lindquist, N. C.; Oh, S.-H. Template-Stripped Asymmetric Metallic Pyramids for Tunable Plasmonic Nanofocusing. *Nano Lett.* **2013**, *13*, 5635–5641.
22. Johnson, T. W.; Lapin, Z. J.; Beams, R.; Lindquist, N. C.; Rodrigo, S. G.; Novotny, L.; Oh, S.-H. Highly Reproducible Near-Field Optical Imaging with Sub-20-nm Resolution Based on Template-Stripped Gold Pyramids. *ACS Nano* **2012**, *6*, 9168–9174.
23. Lee, K.-L.; Chen, P.-W.; Wu, S.-H.; Huang, J.-B.; Yang, S.-Y.; Wei, P.-K. Enhancing Surface Plasmon Detection Using Template-Stripped Gold Nanoslit Arrays on Plastic Films. *ACS Nano* **2012**, *6*, 2931–2939.
24. Desireddy, A.; Conn, B. E.; Guo, J. S.; Yoon, B.; Barnett, R. N.; Monahan, B. M.; Kirschbaum, K.; Griffith, W. P.; Whetten, R. L.; Landman, U.; *et al*. Ultrastable Silver Nanoparticles. *Nature* **2013**, *501*, 399–402.
25. Zhang, Q.; Ge, J. P.; Pham, T.; Goebl, J.; Hu, Y. X.; Lu, Z. D.; Yin, Y. D. Reconstruction of Silver Nanoplates by UV Irradiation: Tailored Optical Properties and Enhanced Stability. *Angew. Chem., Int. Ed.* **2009**, *48*, 3516–3519.
26. Adams, D.; Alford, T. L.; Mayer, J. W. Silver Metallization Stability and Reliability. In *Engineering Materials and Processes*; Springer-Verlag London Ltd: London, UK, 2008; pp 3−16.
27. Krishna, H.; Shirato, N.; Favazza, C.; Kalyanaraman, R. Pulsed Laser Induced Self-Organization by Dewetting of Metallic Films. *J. Mater. Res.* **2011**, *26*, 154–169.
28. Thürmer, K.; Williams, E. D.; Reutt-Robey, J. E. Dewetting Dynamics of Ultrathin Silver Films on Si (111). *Phys. Rev. B* **2003**, *68*, 155423.
29. Yu, H. B.; Jiang, C. S.; Ebert, P.; Wang, X. D.; White, J. M.; Niu, Q.; Zhang, Z. Y.; Shih, C. K. Quantitative Determination of the Metastability of Flat Ag Overlayers on GaAs (110). *Phys. Rev. Lett.* **2002**, *88*, 016102.
30. Krishna, H.; Sachan, R.; Strader, J.; Favazza, C.; Khenner, M.; Kalyanaraman, R. Thickness-Dependent Spontaneous Dewetting Morphology of Ultrathin Ag Films. *Nanotechnology* **2010**, *21*, 155601.
31. Gentili, D.; Foschi, G.; Valle, F.; Cavallini, M.; Biscarini, F. Applications of Dewetting in Micro- and Nanotechnology. *Chem. Soc. Rev.* **2012**, *41*, 4430–4443.
32. Kim, H. C.; Alford, T. L.; Allee, D. R. Thickness Dependence on the Thermal Stability of Silver Thin Films. *Appl. Phys. Lett.* **2002**, *81*, 4287–4289.
33. Chou, C. H.; Lin, C. L.; Chuang, Y. C.; Bor, H. Y.; Liu, C. Y. High Thermally Stable Ni/Ag(Al) Alloy Contacts on p-GaN. *Appl. Phys. Lett.* **2007**, *90*, 022103.
34. Smith, P. H.; Gurev, H. Silicon Dioxide as a High Temperature Stabilizer for Silver Films. *Thin Solid Films* **1977**, *45*, 159–168.
35. Adams, D.; Alford, T. L. Encapsulated Silver for Integrated Circuit Metallization. *Mater. Sci. Eng. R* **2003**, *40*, 207–250.
36. Berthier, S.; Peiro, J.; Fagnent, S.; Gadenne, P. Infrared Absorption of Granular Metal Films in the Percolation Range. *Phys. A (Amsterdam, Neth.)* **1997**, *241*, 1–5.
37. Wang, Y. L.; Nan, F.; Liu, X. L.; Zhou, L.; Peng, X. N.; Zhou, Z. K.; Yu, Y.; Hao, Z. H.; Wu, Y.; Zhang, W.; *et al*. Plasmon-Enhanced Light Harvesting of Chlorophylls on Near-Percolating Silver Films *via* One-Photon Anti-Stokes Upconversion. *Sci. Rep.* **2013**, *3*, 1861.
38. Ding, S.; Wang, X.; Chen, D. J.; Wang, Q. Q. Optical Percolation and Nonlinearity of Sputtered Ag Island Films. *Opt. Express* **2006**, *14*, 1541–1546.
39. Zhang, C.; Zhao, D. W.; Gu, D. E.; Kim, H.; Ling, T.; Wu, Y. K. R.; Guo, L. J. An Ultrathin, Smooth, and Low-Loss Al-Doped Ag Film and Its Application as a Transparent Electrode in Organic Photovoltaics. *Adv. Mater.* **2014**, 10.1002/adma.201306091.
40. Guo, Y.; Jacob, Z. Thermal Hyperbolic Metamaterials. *Opt. Express* **2013**, *21*, 15014–15019.
41. Sree Harsha, K. S. S. *Principles of Physical Vapor Deposition of Thin Films*, 1st ed.; Elsevier Ltd: Oxford, UK, 2006; pp 722−726.

42. Galhenage, R. P.; Yan, H.; Tenney, S. A.; Park, N.; Henkelman, G.; Albrecht, P.; Mullins, D. R.; Chen, D. A. Understanding the Nucleation and Growth of Metals on $TiO_2$: Co Compared to Au, Ni, and Pt. *J. Phys. Chem. C* **2013**, *117*, 7191–7201.
43. Diebold, U.; Pan, J. M.; Madey, T. E. Ultrathin Metal Film Growth on $TiO_2$ (110): an Overview. *Surf. Sci.* **1995**, *331−333*, 845–854.
44. Ali, M. K. M.; Ibrahim, K.; Mkawi, E. M. Ag-Al Alloy Thin Film on Plastic Substrate by Screen Printing for Solar Cell Back Contact Application. *Mater. Sci. Semicond. Process.* **2013**, *16*, 593–597.
45. Waterhouse, G. I. N.; Bowmaker, G. A.; Metson, J. The Thermal Decomposition of Silver (I, III) Oxide: A Combined XRD, FT-IR and Raman Spectroscopic Study. *Phys. Chem. Chem. Phys.* **2001**, *3*, 3838–3845.
46. Gnanavel, M.; Mohan, D. B.; Sunandana, C. S. Optics of Quasi-Particle Phase Transitions in Nanostructured Ag Thin Films. *Thin Solid Films* **2008**, *517*, 1058–1062.